Oxidative tissue injury in multiple sclerosis is only partly reflected in experimental disease models

Acta Neuropathologica

Schuh C[1], Wimmer I[1], Hametner S[1], Van Dam A-M[2], Liblau RS[3], Smith KJ[4], Probert L[5], Binder CJ[6], Bauer J[1], Bradl M[1], Mahad DH[7], Lassmann H[1]

All correspondence to:
Prof. Dr. Hans Lassmann
Department of Neuroimmunology
Centre for Brain Research
Medical University of Vienna
Austria
e.mail: hans.lassmann@meduniwien.ac.at

Supplementary data on investigated material and experimental design:

Human Autopsy Tissue:

The aim of the present study was to compare the extent of oxidative injury between lesions seen in multiple sclerosis (MS) patients and in experimental rodent models of (inflammatory) demyelination. In previous studies, we have analysed oxidative injury [10] and related gene expression. [6,7]. Furthermore, we have studied iron accumulation in relation to pathological alterations [11]. This was all performed on archival tissue from a total of 17 control patients without neurological disease and CNS lesions and 31 patients with MS, including Marburg's type of acute MS, RRMS, SPMS and PPMS. Detailed information on demographics and the clinical courses are provided in the respective publications. For our present study, we selected for direct comparison those cases, which had at least one actively demyelinating lesion as defined below. Demographics and clinical data are provided in Supplementary Table 1:

Supplementary Table 1: Demographics and clinical data of MS patients

	ACMS n = 7	RRMS n = 3	SPMS n = 12	PPMS n = 9	Controls n = 17
Age in years	51 (34 – 78)	47 (40 – 57)	56 (34 – 81)	63 (34 – 83)	57 (30 – 97)
Female / male ratio	5:2	3:0	8:4	7:2	10:7
Disease duration in months	1.7 (0.2 – 4)	179.0 (120 - 262)	279.4 (96 - 444)	195.0 (60 - 372)	--
EDSS	10.0	6 (2.0 – 7.0)	8.0 (4.0 – 9.5)	8.5 (5.0 – 9.5)	--

Besides basic neuropathological classification for inflammation, demyelination and neurodegeneration, these cases were analysed for markers for oxidative injury (oxidised phospholipids (E06 immunoreactivity), malonedialdehyde (MDA2) and 8 hydroxy-deoxyguanosine (8OHdG, [10]); for expression of enzymes involved in oxygen and nitric oxide radical production (NOX1, gp91phox, p22phox, p47phox, NOXO1 and iNOS; [6,7]), for macrophage and microglia activation (CD68, Iba-1; [6,11] and for iron (diaminobenzidine (DAB)-enhanced Turnbull blue staining; [11]). Cellular co-localization of oxidised epitopes, radical producing enzymes and iron were performed by double staining with cell specific markers (oligodendrocytes: TPPP/p25 and CNPase), astrocytes (GFAP), neurons and axons (neurofilament) and microglia (CD68 and Iba-1; [6,7,10,11]).

For direct comparison with animal models, as performed in our present study, we concentrated on those markers, which gave the most distinct and reproducible results in human MS tissue and also showed reproducible and distinct staining with comparable sensitivity to human tissue in inflamed rodent brains (E06 for oxidised phospholipids; p22phox for NADPH oxidase, inducible nitric oxide synthase (iNOS) and iron reactivity with the DAB-enhanced Turnbull blue reaction, see also supplementary material and methods). To ensure comparability of the staining reaction in human and rodent tissue, we always included human MS and/or stroke lesions as positive control, when rodent tissue was stained.

Relevant for our comparison with rodent animal models it has to be emphasized that extensive oxidative injury, reflected by the presence of oxidised lipids and DNA and the expression of

NADPH oxidase, as well as iron accumulation has been already observed in patients with acute MS with a disease duration between 14 days and 2 months [10,11] .

Animal Models:

Acute EAE induced by passive transfer of MBP-reactive $CD4^+$ Th1 T cells:

Lewis rats were bred and housed under standardized conditions in the Decentral Facilities of the Institute for Biomedical Research at the Medical University of Vienna. All animals had access to food and water *ad libitum*. The experiments were approved by the ethic commission of the Medical University of Vienna and performed with the license of the Austrian Ministry for Science and Research.

Experimental autoimmune encephalomyelitis (EAE) was induced by passive transfer (intraperitoneal injection) of $4.5x10^6$ myelin basic protein (MBP)-reactive T cells in young (2 months) and aged (14 months) female Lewis rats. In both groups of animals, disease started 3 to 4 days after T cell transfer with inflammation, which was most pronounced in the lumbar spinal cord. The peak of disease and inflammation was reached on day 6 and declined during the following days. CNS inflammation was characterised by T cell infiltration associated with pronounced microglial activation and peripheral blood monocyte/macrophage recruitment, as shown before in bone marrow chimeric animals [12]. Clinical disease was mainly associated with axonal injury, whereas demyelination was sparse [1]. Animals recovered completely between day 12 and 15 and pathology at this time point revealed only few perivascular inflammatory infiltrates. In the present study, lumbar spinal cord tissue was analysed 6 and 12 days after T cell transfer.

Chronic relapsing EAE in C57BL/6 mice induced by active sensitization with MOG_{35-55} peptide:

Young female adult C57BL/6 mice were actively immunised with 40 μg of rat MOG_{35-55} peptide in complete Freund's adjuvant. Mice also received an intraperitoneal injection of 200 ng of

pertussis toxin (Sigma-Aldrich) on days 0 and 2 post immunization [24]. Clinical disease started at day 10 after immunization and gradually increased over the next 20 days. During the early disease stages (days 10–18), pathology was dominated by perivenous inflammation by T cells associated with microglial activation and macrophage infiltration. Confluent demyelinating destructive lesions developed around day 20 and increased in size and incidence until day 34. Demyelination was associated with extensive axonal injury and loss. For the present study, animals were sampled for pathological analysis on days 21, 27 and 34.

Chronic relapsing EAE in DA rats induced by active sensitization with MOG_{1-125} peptide:

Chronic relapsing EAE was induced by active sensitization with 50 μg myelin oligodendrocyte glycoprotein (MOG_{1-125}) in complete Freund's adjuvant in female and male dark agouti (DA) rats[22]. In the first bout of the disease, perivenous and subpial inflammation by T cells, macrophages and granulocytes was associated with perivenous and subpial demyelination. In the chronic stage, besides initial perivenous lesions as described above, large confluent plaques of demyelination with loss of oligodendrocytes and a variable extent of axonal injury were observed. Furthermore, within the same animal actively demyelinating lesions were seen side by side with inactive demyelinated plaques. In this model, inflammation is triggered by encephalitogenic MOG-reactive $CD4^+$ T cells. Demyelination is induced by demyelinating anti-MOG antibodies, which destroy myelin in parallel through complement activation and antibody dependent cellular cytotoxicity [18,19]. For our study, we selected from a large pool of pathological material animals from chronic relapses (40 to 90 days after sensitization), which all contained actively demyelinating lesions (for definition and staging see below) together with early perivenous lesions and inactive demyelinated plaques.

Acute $CD8^+$ T cell-mediated EAE

Acute demyelinating encephalomyelitis was induced by passive transfer of $3x10^7$ hemagglutinin-reactive $CD8^+$ T cells into female transgenic BALB/c mice expressing hemagglutinin

specifically in oligodendrocytes [21]. In this model, the onset of disease is variable, ranging from day 9 to day 30 after transfer. At any time point within this time window, new actively demyelinating lesions with partial axonal preservation may develop. Thus, at later time points active and inactive lesions are seen in the central nervous system side by side. Active demyelinating lesions are characterised by inflammation, with dominant infiltrates by $CD8^+$ T cells and numerous ramified phagocytic cells showing a microglial morphology. Active demyelination is associated with infiltration of the tissue with granzyme B and $CD8^+$ T cells, which closely attach to oligodendrocytes. Oligodendrocyte destruction is mediated through apoptosis, followed by demyelination [21]. In addition, abundant activated microglia and macrophage-like cells are present in the lesions, which may further contribute to tissue injury. In our present study, we selected brain and spinal cord tissue, containing actively demyelinating lesions from mice sampled between 9 and 28 days after T cell transfer.

LPS injection-induced inflammation

Acute demyelinating myelitis was established by focal injection of 0.5 μl lipopolysaccharide (LPS; 100 ng/μl in saline) into the dorsal column of the spinal cord of adult male Sprague Dawley (SD) rats [5,16], leading to focal inflammation in the dorsal column 12 to 24 hours after LPS injection. Inflammatory infiltrates at this stage of lesions were composed mainly of granulocytes, as well as some T cells and macrophages. This inflammatory phase was followed by a demyelinating phase giving rise to focal demyelinated lesions with relative axonal preservation. This was associated with massive microglia activation and macrophage recruitment starting around day 5 to 7 after focal LPS injection. The peak of active demyelination occurred between 9 and 12 days after injection. For our studies, tissue derived from the inflammatory (0.8-3 days after injection) as well as the demyelinating phase of the disease (5-15 days after injection) was used. Control animals were injected with saline instead of LPS and sampled likewise.

Cuprizone-induced demyelination

Active demyelination was induced by a 0.2% cuprizone (bis-cyclohexanone oxaldihydrazone)-supplemented diet in 8 weeks old male and female *C57BL*/6 mice [25]. Under continuous cuprizone containing diet, the animals developed slowly progressive demyelination starting around day 10. Profound active demyelination was found 35 days after the initiation of the cuprizone diet, which involved large parts of the corpus callosum, the periventricular white matter and also extended into the deeper cortical layers. In our present study, this stage of active demyelination was sampled for further analysis.

Mouse hepatitis virus strain JHM (MHV-JHM) coronavirus-mediated demyelinating disease

Chronic inflammatory demyelinating disease was established by intra-cerebral infection of 4 to 5 week old female Lewis rats with 800 plaque forming units of MHV-JHM coronavirus [2,13,26,27]. This resulted in an acute inflammatory disease mainly affecting the grey matter of the CNS with pronounced virus antigen expression in neurons, astrocytes and oligodendrocytes. Other animals showed a late-onset type of disease, starting around day 30 after virus infection. Pathologically this was reflected either by a chronic panencephalitis affecting grey and white matter, or a chronic inflammatory demyelinating encephalomyelitis mainly involving the brain stem and the spinal cord white matter. The virus antigen was primarily seen in glia cells at these stages of the disease [27]. In the present study, we analysed animals with active lesions from chronic disease stages [2] .

Control animals

In order to validate the stainings, brain, spinal cord and lymphatic tissues of young and aged Lewis rats, SD rats (untreated and saline injected), DA rats and *C57BL*/6 mice without inflammatory lesions were analysed.

Supplementary Table 2: Experimental models:

Model	Animals	Sex	Age	Days of sampling	# of animals	Pathology	# active lesions	# inactive lesions
PT CD4 EAE	Lewis rats	f	Young adult Aged	6, 12 6, 12	14	Diffuse inflammation	0	0
CR MOG35-55 EAE	C56BL/6 mice	f	Young adult	21, 27, 35	5 per time point	Focal Demyelination	109	29
CR MOG1-125 EAE	DA rats	m + f	Young adult	40 to 90	14	Focal demyelination	126	81
PT CD8 EAE	BALB/c mice	f	Young adult	9 to 30	6	Focal demyelination	99	0
LPS	SD rats	m	Adult	0.8 to 3 5 to 15	9 10	Inflammation Focal demyelination	0 8	0 2
Cuprizone	C57BL/6 mice	m + f	Young adult	35	5	Focal demyelination	5	0
Corona Virus	Lewis rats	f	Young adult	30 to 60	11	Focal demyelination	57	40

Passive transfer (PT), chronic (CR); young adult: 1.5 to 3 months old; adult: 4-6 months old; aged: 14 months old; days of sampling: days after disease induction; active lesions: lesions with macrophages with earliest myelin degradation products; inactive lesions: demyelinated sclerotic plaques;

Selection of experimental animals and lesions:

Oxidative injury in multiple sclerosis is associated with inflammation, microglia activation and active demyelination or neurodegeneration and is most pronounced in brain areas with active lesions or ongoing axonal or neuronal degeneration [6,7,10]. To test its potential pathogenic role for demyelination and neurodegeneration in the respective animal models, we concentrated on lesions with inflammation, mediated by different components of the immune system and on lesions with active demyelination or axonal and neuronal injury. Since in individual animals such lesions are present in variable incidence in the chronic stage of the disease, we selected from a much larger pool of animals and tissue blocks those, which still showed signs of active demyelination (for definition see below) or axonal injury, determined by the presence of axons with accumulation of amyloid precursor protein as a sign of acutely impaired fast axonal transport. As active lesions in these animals occur side by side with inactive lesions this sampling strategy also allowed to compare different lesion stages, such as initial lesions, classical active lesions and inactive lesions. Thus, our

selection strategy for further detailed analysis was based on the presence of the entire pathological spectrum of different lesion stages rather than on the time points after disease induction.

Definition of lesion stages and activity of demyelination and neurodegeneration:

For classification of lesional activity, we applied the criteria extensively defined in MS lesions [4,15]. Actively demyelinating lesions were identified by the presence of abundant numbers of macrophages containing myelin degradation products. In early active lesions, the myelin degradation products showed immune-reactivity for all myelin proteins, including myelin oligodendrocyte glycoprotein. Furthermore, early active lesions were surrounded by a rim of microglia activation, only few of them containing sparse myelin protein-reactive intra-cytoplasmic granules (initial lesions, [15]). These lesions showed initial stages of demyelination and oligodendrocyte apoptosis (pre-phagocytic lesions; [3]). Late active lesions contained macrophage inclusions reactive for major myelin proteins, such as myelin basic protein or proteolipid protein. In later stages of lesion development, myelin proteins were degraded in macrophages, which were still abundantly present in the lesions but only contained lipid remnants of myelin. Completely inactive lesions were sharply demarcated from the surrounding normal appearing white matter and showed complete demyelination and astrocytic scaring in the absence of macrophages with myelin degradation products. Acute axonal injury, reflected by APP positive axons, was profound in early and late active lesions but only sparse in the inactive plaque center.

In patients, who died during the progressive stage of the disease, such classical active lesions were rare. The majority of lesions were chronic inactive plaques. In addition, however, a variable number of lesions showed changes, suggesting a slow expansion of pre-existing lesions [14]. Such lesions were characterised by a dense rim of activated microglia at the lesion edge together with some cells with macrophage phenotype, which contained early myelin degradation products. The

number of such macrophages with early myelin degradation products was variable between different plaques, apparently reflecting the degree of ongoing demyelinating activity [14,15].

Lesion staging within the multiple sclerosis tissue blocks was first performed in studies on inflammation [9] and demyelination [14] by the first authors and the senior author of the respective publications. In the subsequent studies on oxidative injury and iron deposition, the classification of the activity stage of lesions was re-evaluated by the principal investigators (LH and SH), since the exact areas of activity may change in some blocks, when multiple serial sections are taken. Thus, each lesion was classified by at least 4 to 5 investigators. Active inflammatory demyelinating lesions in experimental rodent models showed a lesion architecture, which was comparable to that in human MS lesions, and thus allowed to apply the same criteria for lesional staging. The respective blocks were first selected according to lesional activity documented in the neuropathological protocols from the original studies. Then, new sections were cut and the original classification was confirmed by CS and HL in the present study.

Supplementary Methods and Data:

Oxidative damage

In vitro oxidation of native fresh frozen tissue sections

Although the antibody recognising the E06 epitope (oxidised phospholipids) had been used before in rodent tissue, we tested if the epitope could be produced and detected with similar sensitivity and specificity in rodent tissue in our experimental settings (Supplementary Fig.1). Wild-type Lewis rats were perfused with phosphate buffer and brains were snap-frozen in pre-cooled isopentane. Sections (7 µm) were cut and stored at -20 °C. For producing the E06 epitope, we used iron-induced oxidative damage *in vitro*. For Fe^{2+}/ascorbate and H_2O_2-induced lipid peroxidation [20,23], the sections were treated over night at 37 °C with 20 µM $FeSO_4$ (Merck) and 1 mM ascorbate (Sigma Aldrich) and 500 µM tbH_2O_2 (Luperox Sigma Aldrich). Prior to staining for E06, slides were

fixed with acetone/PFA and the staining was performed as described in the materials and methods part of the main manuscript.

Iron

Validation of DAB-enhanced Turnbull blue staining (TBB) with ferrozene assay

For methodological reasons, we compared the iron content of rat cerebella at different ages using two different techniques: the DAB-enhanced Turnbull blue staining (TBB) as an established histological detection of iron [17] and the ferrozene assay [8] for biochemical iron quantification of fresh tissue. We stained cerebella of rats from the age of 2 to 20 months using the TBB protocol and analysed the optical density of pictures taken from the dentate nucleus, which shows iron accumulation in the TBB staining with increasing age. Similarly, we quantified iron of whole rat cerebella using the ferrozene assay. We found a linear correlation (r = 0.485, p < 0.001) when we compared the optical density of TBB stained slides with the iron concentration in cerebella (Supplementary Fig. 2).

Iron quantification

Rats aged from 2 to 20 months were sacrificed and perfused with phosphate buffer. Cerebella were homogenised in sodium potassium phosphate buffer (5 mM, pH = 7.4). The iron content of rat cerebella was determined using the colorimetric ferrozene assay [8]. Iron was released from proteins and stable iron complexes by acidic permanganate treatment at 60 °C for 2 hours. Subsequently, iron was reduced by ascorbic acid to Fe^{2+} and quantitatively complexed by ferrozene. In order to catch interfering copper ions, neocuproine was added to the reaction. Absorption was measured at 540 nm using a Powerwave X-340 plate reader. Data were normalised to protein concentration determined by total protein measurement using a Nanodrop 2000 spectrophotometer. Iron accumulation in rat brain tissue detected by the DAB-enhanced Turnbull reaction correlated significantly with the iron content in the tissue determined by biochemical analysis of total iron content (Supplementary Fig.2).

Supplementary Figures

Supplementary Figure 1: Optical density of E06 after *in vitro* oxidation. The epitope of E06 could be detected in rat tissue after in vitro oxidation of frozen native brain sections using iron containing free-radical generating systems. After staining for E06, the optical density of oxidised phospholipids in iron-treated sections was higher than in control sections (n = 6, $p \leq 0.001$, indicated by ***)

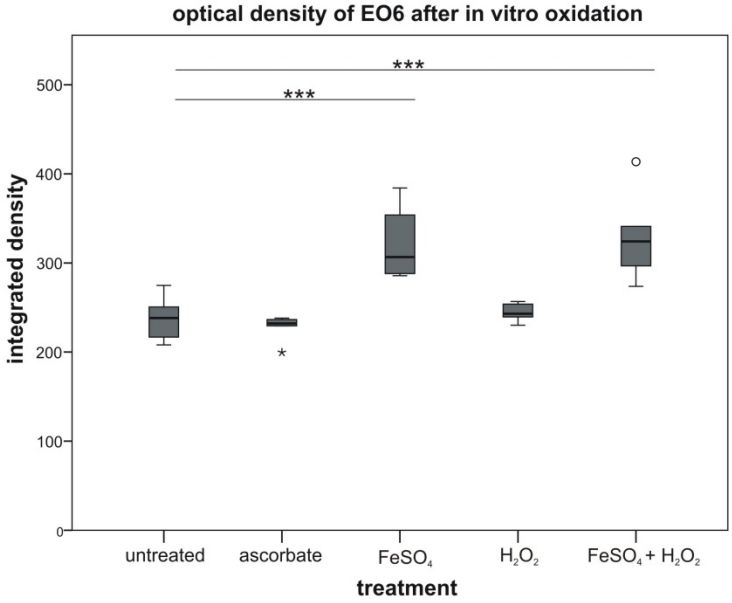

Supplementary Figure 2: Histochemistry correlates with biochemical iron quantification: comparison of DAB-enhanced Turnbull blue staining (x-axis) with iron concentration determined by ferrozene assay (y-axis) of rat cerebella from animals aged 2 to 20 months (n = 52, $r = 0.485$, $p < 0.001$).

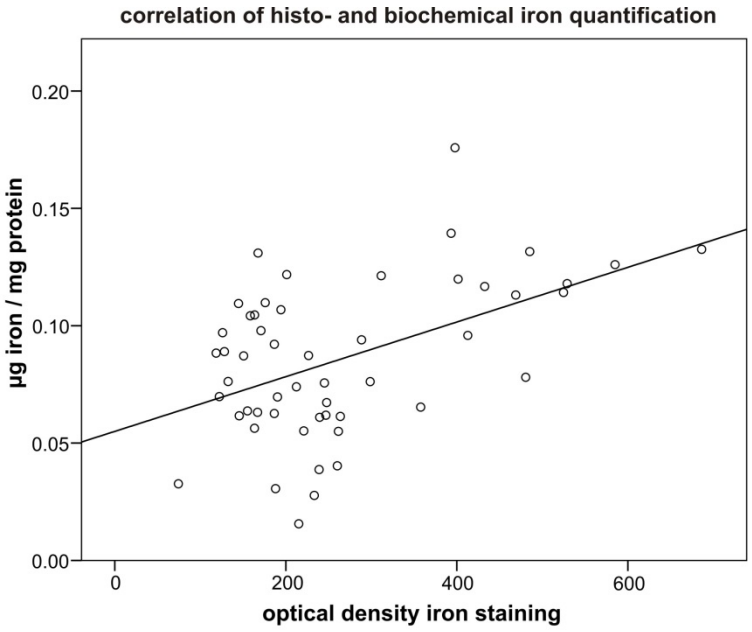

Supplementary Table 3: Details on the investigated genes and Agilent whole-genome microarray probes used for the gene expression study in human multiple sclerosis tissue

Gene symbol	Gene name	Accession number	Probe ID
Oxidative stress			
Sod1	Superoxide dismutase 1, soluble	NM_000454	A_23_P154840 A_24_P151464
Sod2	Superoxide dismutase 2, mitochondrial, transcript variant 2	NM_001024465	A_23_P134176
Sod3	Superoxide dismutase 3, extracellular	NM_003102	A_23_P254741
Nos1	Nitric oxide synthase 1 (neuronal), transcript variant 1	NM_000620	A_24_P934355 A_23_P204791
Nos1	Nitric oxide synthase 1 (neuronal), transcript variant 2	NM_001204218	A_32_P332320
Nos2	Nitric oxide synthase 2, inducible	NM_000625	A_23_P502464
Nos3	Nitric oxide synthase 3 (endothelial cell), transcript variant 1	NM_000603	A_23_P70849
Nox1	NADPH oxidase 1, transcript variant NOH-1L	NM_007052	A_23_P217280 A_23_P316410
Nox1	NADPH oxidase 1, transcript variant NOH-1Lv	NM_013955	A_23_P304921
Cybb	Cytochrome b-245, beta polypeptide	NM_000397	A_23_P217258 A_24_P365767
Nox3	NADPH oxidase 3	NM_015718	A_23_P82099
Cyba	Cytochrome b-245, alpha polypeptide	NM_000101	A_23_P163506
Ncf1	Neutrophil cytosolic factor 1	NM_000265	A_23_P42746 A_32_P116203
Ncf2	Neutrophil cytosolic factor 2, transcript variant 1	NM_000433	A_23_P138194
Ncf4	Neutrophil cytosolic factor 4, 40kDa, transcript variant 1	NM_000631	A_23_P109508
Noxa1	NADPH oxidase activator 1	NM_006647	A_23_P254353
Noxo1	NADPH oxidase organizer 1, transcript variant a	NM_144603	A_23_P413051
Cat	Catalase	NM_001752	A_23_P105138
Gpx1	Glutathione peroxidase 1, transcript variant 2	NM_201397	A_23_P250671
Gpx2	Glutathione peroxidase 2 (gastrointestinal)	NM_002083	A_23_P3038
Mpo	Myeloperoxidase	NM_000250	A_23_P141173
Iron metabolism			
FtH1	Ferritin, heavy polypeptide 1	NM_002032	A_24_P58337 A_24_P919330 A_32_P111565 A_32_P820503 A_32_P342064
FtL	Ferritin, light polypeptide	NM_000146	A_32_P155247 A_23_P50498 A_23_P50504
FtMt	Ferritin mitochondrial	NM_177478	A_32_P160896 A_23_P367596
Tf	Transferrin	NM_001063	A_23_P212500 A_23_P212508
Tfrc	Transferrin receptor (p90, CD71), transcript variant 1	NM_003234	A_23_P212617
Scara5	Scavenger receptor class A, member 5 (putative)	NM_173833	A_23_P94103 A_23_P372386
Slc11a2	Solute carrier family 11 (proton-coupled divalent metal ion transporters), member 2, transcript variant 4	NM_000617	A_24_P381494 A_23_P139820
Slc39a14	Solute carrier family 39 (zinc transporter), member 14, transcript variant 2	NM_015359	A_24_P383356 A_23_P59950 A_24_P333479
Slc39a8	Solute carrier family 39 (zinc transporter), member 8 (SLC39A8), transcript variant 1	NM_022154	A_23_P41424
Trpc6	Transient receptor potential cation channel, subfamily C, member 6	NM_004621	A_23_P127547

Slc11a1	Solute carrier family 11 (proton-coupled divalent metal ion transporters), member 1	NM_000578	A_24_P88690 A_23_P39665 A_24_P76831
Cybrd1	Cytochrome b reductase 1, transcript variant 1	NM_024843	A_23_P209564 A_24_P345451
Slc40a1	Solute carrier family 40 (iron-regulated transporter), member 1	NM_014585	A_23_P102391
Cp	Ceruloplasmin (ferroxidase)	NM_000096	A_23_P414793
Heph	Hephaestin, transcript variant 2	NM_014799	A_24_P399980 A_23_P22526
Mon1a	MON1 homolog A (yeast), transcript variant 1	NM_032355	A_23_P41075
Hamp	Hepcidin antimicrobial peptide	NM_021175	A_23_P165162
Mitochondrially-encoded			
Mt-Nd1	Mitochondrially encoded NADH dehydrogenase 1	ENST00000361390	A_23_P331028 A_24_P182122
Mt-Nd2	Mitochondrially encoded NADH dehydrogenase 2	ENST00000361453	A_23_P431853
Mt-Nd3	Mitochondrially encoded NADH dehydrogenase 3	ENST00000361227	A_23_P360209 A_23_P360213
Mt-Nd4	Mitochondrially encoded NADH dehydrogenase 4	ENST00000361381	A_23_P315252 A_24_P710024
Mt-Nd5	Mitochondrially encoded NADH dehydrogenase 5	ENST00000361567	A_23_P406928
Mt-Nd6	Mitochondrially encoded NADH dehydrogenase 6	ENST00000361681	A_23_P317056
Mt-Co1	Mitochondrially encoded cytochrome c oxidase I	ENST00000361624	A_23_P301925
Mt-Co2	Mitochondrially encoded cytochrome c oxidase II	ENST00000361739	A_23_P402751
Mt-Co3	Mitochondrially encoded cytochrome c oxidase III	ENST00000362079	A_24_P350200
Mt-Atp6	Mitochondrially encoded ATP synthase 6	ENST00000361899	A_23_P337726
Mt-Cyb	Mitochondrially encoded cytochrome b	ENST00000361789	A_24_P551842 A_24_P557534
Mitochondria			
Cycs	Cytochrome c, somatic	NM_018947	A_32_P174083 A_24_P29665 A_24_P376556
Cox4i1	Cytochrome c oxidase subunit IV isoform 1	NM_001861	A_23_P141032 A_23_P141029
Bak1	BCL2-antagonist/killer 1	NM_001188	A_23_P145357
Bcl2	B-cell CLL/lymphoma 2, transcript variant alpha	NM_000633	A_23_P352266
Bid	BH3 interacting domain death agonist, transcript variant 1	NM_197966	A_23_P154929 A_24_P187948
Ucp1	Uncoupling protein 1 (mitochondrial, proton carrier)	NM_021833	A_23_P30091
Ucp2	Uncoupling protein 2 (mitochondrial, proton carrier)	NM_003355	A_23_P47704
Ucp3	Uncoupling protein 3 (mitochondrial, proton carrier), transcript variant short	NM_022803	A_24_P292470
Ucp3	Uncoupling protein 3 (mitochondrial, proton carrier), transcript variant long	NM_003356	A_23_P203601
Cdkn2a	Cyclin-dependent kinase inhibitor 2A (melanoma, p16, inhibits CDK4), transcript variant 3	NM_058197	A_23_P43490 A_23_P43484
Tspo	Translocator protein (18kDa), transcript variant PBR	NM_000714	A_24_P134526
Tp53	Tumor protein p53 (TP53), transcript variant 1	NM_000546	A_23_P26810
Fxn	Frataxin, transcript variant 2	NM_181425	A_23_P60517

Supplementary Table 4: Details on the investigated genes and applied TaqMan® assays for the gene expression study in rat tissue

Gene symbol	Gene name	Accession number	TaqMan® assay ID
Oxidative stress			
Sod1	Superoxide dismutase 1, soluble	NM_017050	Rn00566938_m1
Sod2	Superoxide dismutase 2, mitochondrial	NM_017051	Rn00690588_g1
Sod3	Superoxide dismutase 3, extracellular	NM_012880	Rn00563570_m1
Nos1	Nitric oxide synthase 1, neuronal	NM_052799	Rn00583793_m1
Nos2	Nitric oxide synthase 2, inducible	NM_012611	Rn00561646_m1
Nos3	Nitric oxide synthase 3, endothelial cell	NM_021838	Rn02132634_s1
Nox1	NADPH oxidase 1	NM_053683	Rn00586652_m1
Cybb	Cytochrome b-245, beta polypeptide	NM_023965	Rn00576710_m1
Nox3	NADPH oxidase 3	NM_001004216	Rn01430441_m1
Cyba	Cytochrome b-245, alpha polypeptide	NM_024160	Rn00577357_m1
Ncf1	Neutrophil cytosolic factor 1	NM_053734	Rn00586945_m1
Ncf2	Neutrophil cytosolic factor 2	NM_001100984	Rn01759079_m1
Ncf4	Neutrophil cytosolic factor 4	NM_001127304	Rn01505557_m1
Noxa1	NADPH oxidase activator 1	NM_001100171	Rn01438660_m1
Noxo1	NADPH oxidase organizer 1	NM_001106986	Rn01751547_g1
Cat	Catalase	NM_012520	Rn00560930_m1
Gpx1	Glutathione peroxidase 1	NM_030826	Rn00577994_g1
Gpx2	Glutathione peroxidase 2	NM_183403	Rn00822100_gH
Mpo	Myeloperoxidase	NM_001107036	Rn01460205_m1
Iron metabolism			
FtH1	Ferritin, heavy polypeptide 1	NM_012848	Rn00820640_g1
FtL	Ferritin, light polypeptide	NM_022500	Rn00821071_g1
FtMt	Ferritin, mitochondrial	NM_001106136	Rn01492073_s1
Tf	Transferrin	NM_001013110	Rn01445482_m1
Tfrc	Transferrin receptor	NM_022712	Rn01474701_m1
Scara5	Scavenger receptor class A, member 5 (putative)	NM_001135855	Rn01534922_m1
Slc11a2	Solute carrier family 11 (proton-coupled divalent metal ion transporters), member 2	NM_013173	Rn01533109_m1
Slc39a14	Solute carrier family 39 (zinc transporter), member 14	NM_001107275	Rn01468336_m1
Slc39a8	Solute carrier family 39 (zinc transporter), member 8	NM_001011952	Rn01748352_m1
Trpc6	Transient receptor potential cation channel, subfamily C, member 6	NM_053559	Rn00677559_m1
Slc11a1	Solute carrier family 11 (proton-coupled divalent metal ion transporters), member 1	NM_001031658	Rn02114013_s1
Cybrd1	Cytochrome b reductase 1	NM_001011954	Rn01484657_m1
Slc40a1	Solute carrier family 39 (iron-regulated transporter), member 1	NM_133315	Rn00591187_m1
Cp	Ceruloplasmin	NM_012532	Rn00561049_m1
Heph	Hephaestin	NM_133304	Rn00515970_m1
Mon1a	MON1 homolog A (yeast)	NM_001126284	Rn00511678_m1
Hamp	Hepcidin antimicrobial peptide	NM_053469	Rn00584987_m1
Mitochondrially-encoded			
Mt-Nd1	NADH dehydrogenase 1, mitochondrial	ENSRNOT00000047550	Rn03296764_s1
Mt-Nd2	NADH dehydrogenase 2, mitochondrial	ENSRNOT00000040993	Rn03296765_s1
Mt-Nd3	NADH dehydrogenase 3, mitochondrial	ENSRNOT00000041241	Rn03296825_s1
Mt-Nd4	NADH dehydrogenase 4, mitochondrial	ENSRNOT00000042928	Rn03296781_s1
Mt-Nd4l	NADH dehydrogenase 4L, mitochondrial	ENSRNOT00000044582	Rn03296792_s1
Mt-Nd5	NADH dehydrogenase 5, mitochondrial	ENSRNOT00000048767	Rn03296799_s1
Mt-Nd6	NADH dehydrogenase 6, mitochondrial	ENSRNOT00000051268	Rn03296815_s1
Mt-Co1	Cytochrome c oxidase I, mitochondrial	ENSRNOT00000050156	Rn03296721_s1

Mt-Co3	Cytochrome c oxidase III, mitochondrial	ENSRNOT00000049683	Rn03296820_s1
Mt-Atp6	ATP synthase 6, mitochondrial	ENSRNOT00000046108	Rn03296710_s1
Mt-Atp8	ATP synthase 8, mitochondrial	ENSRNOT00000046201	Rn03296716_s1
Mt-Cytb	Cytochrome b, mitochondrial	ENSRNOT00000042098	Rn03296746_s1
Mitochondria			
Cycs	Cytochrome c, somatic	NM_012839	Rn01410227_g1
Cox4i1	Cytochrome c oxidase subunit IV isoform 1	NM_017202	Rn00665001_g1
Bak1	BCL2-antagonist/killer 1	NM_053812	Rn01429084_m1
Bcl2	B-cell CLL/lymphoma 2	NM_016993	Rn99999125_m1
Bid	BH3 interacting domain death agonist	NM_022684	Rn01459517_m1
Ucp1	Uncoupling protein 1 (mitochondrial, proton carrier)	NM_012682	Rn00562126_m1
Ucp2	Uncoupling protein 2 (mitochondrial, proton carrier)	NM_019354	Rn01754856_m1
Ucp3	Uncoupling protein 3 (mitochondrial, proton carrier)	NM_013167	Rn00565874_m1
Cdkn2a	Cyclin-dependent kinase inhibitor 2A	NM_031550	Rn00580664_m1
Tspo	Translocator protein	NM_012515	Rn00560892_m1
Tp53	Tumor protein p53	NM_030989	Rn00755717_m1
Fxn	Frataxin	NM_001191952	Rn01501404_g1
Reference genes			
18S	Eukaryotic 18S rRNA	X03205	Hs99999901_s1
Gapdh	Gyceraldehyde-3-phosphate dehydrogenase	NM_017008	Rn01775763_g1
Hprt1	Hypoxanthine phosphoribosyltransferase 1	NM_012583	Rn01527840_m1
Pgk1	Phosphoglycerate kinase 1	NM_053291	Rn01474008_gH
Ppia	Peptidylprolyl isomerase A (cyclophilin A)	NM_017101	Rn00690933_m1

References:

1. Aboul-Enein F, Weiser P, Hoftberger R, Lassmann H, Bradl M (2006) Transient axonal injury in the absence of demyelination: a correlate of clinical disease in acute experimental autoimmune encephalomyelitis. Acta Neuropathol 111 (6):539-547. doi:10.1007/s00401-006-0047-y
2. Barac-Latas V, Suchanek G, Breitschopf H, Stuehler A, Wege H, Lassmann H (1997) Patterns of oligodendrocyte pathology in coronavirus-induced subacute demyelinating encephalomyelitis in the Lewis rat. Glia 19 (1):1-12
3. Barnett MH, Prineas JW (2004) Relapsing and remitting multiple sclerosis: pathology of the newly forming lesion. Ann Neurol 55 (4):458-468. doi:10.1002/ana.20016
4. Bruck W, Porada P, Poser S, Rieckmann P, Hanefeld F, Kretzschmar HA, Lassmann H (1995) Monocyte/macrophage differentiation in early multiple sclerosis lesions. Ann Neurol 38 (5):788-796. doi:10.1002/ana.410380514
5. Felts PA, Woolston AM, Fernando HB, Asquith S, Gregson NA, Mizzi OJ, Smith KJ (2005) Inflammation and primary demyelination induced by the intraspinal injection of lipopolysaccharide. Brain 128 (Pt 7):1649-1666. doi:10.1093/brain/awh516
6. Fischer MT, Sharma R, Lim JL, Haider L, Frischer JM, Drexhage J, Mahad D, Bradl M, van Horssen J, Lassmann H (2012) NADPH oxidase expression in active multiple sclerosis lesions in relation to oxidative tissue damage and mitochondrial injury. Brain 135 (Pt 3):886-899. doi:10.1093/brain/aws012
7. Fischer MT, Wimmer I, Hoftberger R, Gerlach S, Haider L, Zrzavy T, Hametner S, Mahad D, Binder CJ, Krumbholz M, Bauer J, Bradl M, Lassmann H (2013) Disease-specific molecular events in cortical multiple sclerosis lesions. Brain 136 (Pt 6):1799-1815. doi:10.1093/brain/awt110
8. Fish WW (1988) Rapid colorimetric micromethod for the quantitation of complexed iron in biological samples. Methods Enzymol 158:357-364
9. Frischer JM, Bramow S, Dal-Bianco A, Lucchinetti CF, Rauschka H, Schmidbauer M, Laursen H, Sorensen PS, Lassmann H (2009) The relation between inflammation and neurodegeneration in multiple sclerosis brains. Brain 132 (Pt 5):1175-1189. doi:10.1093/brain/awp070
10. Haider L, Fischer MT, Frischer JM, Bauer J, Hoftberger R, Botond G, Esterbauer H, Binder CJ, Witztum JL, Lassmann H (2011) Oxidative damage in multiple sclerosis lesions. Brain 134 (Pt 7):1914-1924. doi:10.1093/brain/awr128
11. Hametner S, Wimmer I, Haider L, Pfeifenbring S, Bruck W, Lassmann H (2013) Iron and neurodegeneration in the multiple sclerosis brain. Ann Neurol. doi:10.1002/ana.23974
12. Hickey WF, Vass K, Lassmann H (1992) Bone marrow-derived elements in the central nervous system: an immunohistochemical and ultrastructural survey of rat chimeras. J Neuropathol Exp Neurol 51 (3):246-256
13. Korner H, Schliephake A, Winter J, Zimprich F, Lassmann H, Sedgwick J, Siddell S, Wege H (1991) Nucleocapsid or spike protein-specific CD4+ T lymphocytes protect against coronavirus-induced encephalomyelitis in the absence of CD8+ T cells. J Immunol 147 (7):2317-2323
14. Kutzelnigg A, Lucchinetti CF, Stadelmann C, Bruck W, Rauschka H, Bergmann M, Schmidbauer M, Parisi JE, Lassmann H (2005) Cortical demyelination and diffuse white matter injury in multiple sclerosis. Brain 128 (Pt 11):2705-2712. doi:10.1093/brain/awh641
15. Lassmann H (2011) Review: the architecture of inflammatory demyelinating lesions: implications for studies on pathogenesis. Neuropathol Appl Neurobiol 37 (7):698-710. doi:10.1111/j.1365-2990.2011.01189.x
16. Marik C, Felts PA, Bauer J, Lassmann H, Smith KJ (2007) Lesion genesis in a subset of patients with multiple sclerosis: a role for innate immunity? Brain 130 (Pt 11):2800-2815. doi:10.1093/brain/awm236
17. Meguro R, Asano Y, Odagiri S, Li C, Iwatsuki H, Shoumura K (2007) Nonheme-iron histochemistry for light and electron microscopy: a historical, theoretical and technical review. Arch Histol Cytol 70 (1):1-19

18. Piddlesden S, Lassmann H, Laffafian I, Morgan BP, Linington C (1991) Antibody-mediated demyelination in experimental allergic encephalomyelitis is independent of complement membrane attack complex formation. Clin Exp Immunol 83 (2):245-250
19. Piddlesden SJ, Lassmann H, Zimprich F, Morgan BP, Linington C (1993) The demyelinating potential of antibodies to myelin oligodendrocyte glycoprotein is related to their ability to fix complement. Am J Pathol 143 (2):555-564
20. Ribeiro AS, Souza MO, Scofano HM, Creczynski-Pasa TB, Mignaco JA (2007) Inhibition of spinach chloroplast F0F1 by an Fe2+/ascorbate/H2O2 system. Plant Physiol Biochem 45 (10-11):750-756. doi:10.1016/j.plaphy.2007.07.014
21. Saxena A, Bauer J, Scheikl T, Zappulla J, Audebert M, Desbois S, Waisman A, Lassmann H, Liblau RS, Mars LT (2008) Cutting edge: Multiple sclerosis-like lesions induced by effector CD8 T cells recognizing a sequestered antigen on oligodendrocytes. J Immunol 181 (3):1617-1621
22. Storch MK, Stefferl A, Brehm U, Weissert R, Wallstrom E, Kerschensteiner M, Olsson T, Linington C, Lassmann H (1998) Autoimmunity to myelin oligodendrocyte glycoprotein in rats mimics the spectrum of multiple sclerosis pathology. Brain Pathol 8 (4):681-694
23. Takatsu H, Ogata M, Fukui K, Takeda T, Endo T, Urano S (2009) Inhibitory effect of Lysichiton camtschatcense extracts on Fe2+/ascorbate-induced lipid peroxidation in rat kidney and brain homogenates. J Nat Med 63 (3):364-367. doi:10.1007/s11418-009-0333-9
24. Taoufik E, Tseveleki V, Chu SY, Tselios T, Karin M, Lassmann H, Szymkowski DE, Probert L (2011) Transmembrane tumour necrosis factor is neuroprotective and regulates experimental autoimmune encephalomyelitis via neuronal nuclear factor-kappaB. Brain 134 (Pt 9):2722-2735. doi:10.1093/brain/awr203
25. Van Strien ME, Baron W, Bakker EN, Bauer J, Bol JG, Breve JJ, Binnekade R, Van Der Laarse WJ, Drukarch B, Van Dam AM (2011) Tissue transglutaminase activity is involved in the differentiation of oligodendrocyte precursor cells into myelin-forming oligodendrocytes during CNS remyelination. Glia 59 (11):1622-1634. doi:10.1002/glia.21204
26. Wege H, Schluesener H, Meyermann R, Barac-Latas V, Suchanek G, Lassmann H (1998) Coronavirus infection and demyelination. Development of inflammatory lesions in Lewis rats. Adv Exp Med Biol 440:437-444
27. Zimprich F, Winter J, Wege H, Lassmann H (1991) Coronavirus induced primary demyelination: indications for the involvement of a humoral immune response. Neuropathol Appl Neurobiol 17 (6):469-484